Fermi National Accelerator Laboratory

A New Detector Technique Using Triangular Scintillating Strips to Measure the Position of Minimum Ionizing Particles

M. Adams et al.

For the D0 Collaboration

Fermi National Accelerator Laboratory
P.O. Box 500, Batavia, Illinois 60510

March 1996

Disclaimer

A New Detector Technique Using Triangular Scintillating Strips to Measure the Position of Minimum Ionizing Particles

M. Adams [b], N. Amos [c], D.A. Averill [b], P. Baringer [c,1],
A. Bross [a], M. Chung [b], F. Hsieh [c], H. Li [d], D. Lincoln [c,3],
S. Margulies [b,2], H. Neal [c], E. Neis [c], L. Oesch [c], J. Qian [c],
M. Rijssenbeek [d]

[a] *Fermi National Accelerator Laboratory, Batavia, Illinois 60510, USA*

[b] *University of Illinois at Chicago, Chicago, Illinois 60607, USA*

[c] *University of Michigan, Ann Arbor, Michigan 48109, USA*

[d] *State University of New York, Stony Brook, New York 11794, USA*

(for the DØ Collaboration)

We present a new technique for measuring the position where a charged particle transits a detector which achieves a position resolution much better than the granularity of the detector. This is accomplished by using scintillating strips with a triangular cross-section and an axial wavelength shifting fiber readout. We tested strips with a base of 9 mm and a height of 4.5 mm and achieved a position resolution of 567 μm. With over 60 000 cosmic ray data points per strip, we are able to precisely characterize the performance of this detector design. In addition, we offer suggestions for future improvements in the achievable position resolution. Additional performance results, including uniformity and yield, are also discussed.

---

[1] Visitor from *University of Kansas, Lawrence, Kansas 66045, USA*
[2] Deceased
[3] Corresponding author. Tel. +1 708 840 5218, email fnal::lucifer, lucifer@fnal.fnal.gov

1 Introduction

Hodoscopes manufactured from scintillating plastic strips or panels have long been used to measure the position where charged particles cross them. In order to improve the position resolution of such a detector, it is necessary to decrease the size of each strip. As the ratio of the strip's length to its transverse dimension increases, the attenuation length of the strip decreases and it becomes increasingly difficult to achieve a useful signal. By combining the technologies of scintillating plastic and optical fiber, it is possible to extend this hodoscope technique to very small transverse dimensions [1]. As an example, the DØ fiber group has made ribbons from 835 μm scintillating fiber. By using two ribbons, staggered by half a fiber, position resolutions of ~ 100 μm have been achieved.

In most instances, the position where a particle crosses a hodoscope is determined merely by knowing which strip or combination of strips is crossed. Because of this, improving the resolution requires decreasing the strip size and thus increasing the channel count. Because cost is proportional to channel count, it would be convenient to develop a technique where one could interpolate particle position between adjacent strips. This paper discusses such a technique.

A recent paper [2] has detailed test results of a detector which contained plastic scintillating strips of nearly square cross-section ($5.0 \times 4.5 \times 1000$ mm) with an axial wavelength shifting (WLS) fiber readout. Light from the WLS fibers was piped through long clear fibers to Visible Light Photon Counters (VLPC's). [1] That detector was built as a prototype for a preshower detector which is to be a component of a major upgrade to the DØ detector at Fermilab [4]. In that prototype, the strips were arranged in tiles sixteen strips wide and one strip high. Each strip within a tile was optically separated from its neighbors by white glue 0.8 mm thick. Each tile was wrapped in Tyvek and then several tiles were stacked. The details of a high statistics cosmic ray study of those strips is given in Ref. [2].

The DØ preshower detector must fit into a very limited radial space and also must have excellent position resolution in order to match its signals with charged tracks seen in the central tracking system. The prototype module discussed above performed satisfactorily, but with two obvious limitations. The first is the fact that the white isolation glue was optically dead, thus

---

[1] VLPC's [3] are being developed and tested jointly by Rockwell International and the DØ experiment at Fermilab and are semiconductor devices with typical quantum efficiencies (QE's) of 80% for 540 nm light and typical gains of 50 000. In this study we use an earlier model of the VLPC (HISTE-IV) which has a both a lower QE (65%) and a lower gain (15 000).

necessitating at least two layers to guard against dead regions. The second limitation is the fact that the position resolution of a strip of width a is simply $a/\sqrt{12}$.

Thus a different cross-section strip is considered—that of a triangle. Figure 1 shows how a mega-tile of triangular strips would be constructed. The absence of a dead region (to normally incident particles) is manifest and, as we will show, the position resolution is quite good.

In this paper we report on a detailed study of a cosmic ray test of the triangular cross-section strips, using the same test stand as in Ref. [2]. Light yields, uniformity of response, and position resolution of the prototype device are discussed.

2   Expected Position Resolution with Triangular Strips

Neglecting some effects which will be discussed in a moment, a detector consisting of interlocking triangular scintillating strips (as shown in Fig. 1) can measure the position of a charged particle which crosses it at normal incidence to arbitrary precision. This position can be given by the mathematical expression:

$$x_{\text{vernier}} = x_o \pm a\frac{t_2}{t_1 + t_2} \tag{1}$$

where a is the half-length of the base of the triangle, t_1 is the thickness of scintillator crossed by the charged particle in the strip which is centered at position x_o, and t_2 is the thickness in the adjacent strip. The $\pm$ indicates that the relationship is valid regardless of the relative position of the adjacent strip (either to the right or left).

Equation (1) gives the position (x_{vernier}) of a particle in terms of the path length traversed in two adjacent strips of scintillator. What one actually measures is not t, but the signal from each strip. This signal (S) is related to the thickness of scintillator traversed (t) by the simple relationship $S = kt$, where k is a proportionality constant. Thus, one might replace the t's in eq. (1) with $t = S/k$. However, this equation can perhaps be most clearly expressed by making the following observations. One can use the fact that a particle travelling through the maximum thickness of scintillator (T_{max}) follows the relationship $S_{\text{max}} = kT_{\text{max}}$. One may then write $t = (S/S_{\text{max}})T_{\text{max}}$. Since all of the strips have identical thickness, one may then express eq. (1) as the more

2

convenient:

$$x_{\text{vernier}} = x_o \pm a \frac{S_2/S_2^{\text{max}}}{S_1/S_1^{\text{max}} + S_2/S_2^{\text{max}}} \qquad (2)$$

Details on extracting S^{max} will be given in Sec. (5.3).

Unfortunately, the thickness of scintillator traversed does not solely determine the signal observed. Landau fluctuations in the dE/dx loss, Poisson fluctuations in light collection (and photoelectron generation) and spatially dependent, non-uniform light collection all degrade position resolution. As we will see in Sec. (5.3), the light collection efficiency is quite uniform and thus we discuss the other two effects.

The number of photoelectrons observed per minimum ionizing particle (MIP) is often quite low for scintillator and fiber based detectors, especially those whose photodetector is a conventional photomultiplier. Thus we first address the effects of small-valued, quantized signals. As is evident in Fig. 1, $t_1 + t_2 = T_{\text{max}} = \text{constant}$. Define N to be the average number of photoelectrons generated by a particle traversing T_{max}. The average number of photoelectrons generated in strip #1 is $N_1 = (t_1/T_{\text{max}})N$ and N_2 is similarly defined for strip #2. A simple Monte Carlo was written in which a position x was chosen from a uniform distribution ($0 < x < a$, where $2a$ is the length of the base of the triangle). The two thicknesses t_1 and t_2 were determined, as were N_1 and N_2. The number of photoelectrons observed for each strip was then independently generated (e.g. for strip #1, the number of photoelectrons observed, n_1, was chosen from a Poisson distribution with mean N_1). The signal for each strip was then just the observed number of photoelectrons associated with that strip. Since response factors $k_1 = k_2$ in this model, the measured position x_{vernier} can then be determined

$$x_{\text{vernier}} = x_o + a \frac{n_2}{n_1 + n_2}.$$

Finally, a distribution of the residual ($x_{\text{vernier}} - x_{\text{actual}}$) is formed. Figure 2 shows the RMS of this distribution in units of a as a function of the average total number of photoelectrons (N). Our VLPC readout gives us $N \sim 20$, as discussed below, putting us in the flatter part of this curve.

It is more difficult to formally characterize the effects of Landau fluctuations. However, for a specific geometry this is much easier. For the actual geometry and materials used in this test (discussed below), the energy loss in the two adjacent strips (E_1 and E_2 respectively) was allowed to fluctuate according to Landau theory. Since the average observed light is proportional to energy loss, the average number of photoelectrons in strip #1 is $N_1 = (E_1/ < E_{\text{max}} >)N$,

3

where E_1 and N are defined above and $< E_{\mathrm{max}} >$ is the average energy lost when a particle traverses the maximum thickness of scintillator.

For the very specific case of the strips that we tested (i.e. triangular strips, with height 4.5 mm, base 9 mm, and with yields of 4 photoelectrons per millimeter of scintillator traversed), this Monte Carlo approach gives a position resolution of 450 μm from Poisson statistics alone, 366 μm from Landau fluctuations alone, and 580 μm when the two effects are added in quadrature. A Monte Carlo which includes the correlation between the two effects reduces the final resolution to 560 μm, suggesting the correlation is small.

The degree to which Landau fluctuations smear the expected signal depends on the amount of material traversed. The effect of Poisson fluctuations depends on the quantized nature of the signal and, in a related vein, the efficiency of light and photoelectron production for given energy loss. These effects are not strongly related and thus it is not possible to state in a case-independent way the size of the relative contributions of these two effects.

3 Construction Details

A test module consisting of 128 channels was constructed to investigate the triangular strip design. Since the ultimate purpose of our ongoing R&D effort is to design and construct a preshower detector for the D∅ upgrade [4], certain restrictions not obvious in the context of this test were imposed on the design. In order for the final detector to fit within its allotted radial space budget and have the desired channel count, it is anticipated that the strip cross-section should be a right isosceles triangle (45°-45°-90°) with a base of approximately 9 mm and a height of 4.5 mm. Since scintillating strips of this cross-section have not been tested before, it was decided to test several small variations on the baseline design. An earlier study [2] showed that Bicron [5] BC-404 series scintillator, in conjunction with Kuraray Y-11 [6,7] multi-clad fiber gave acceptable light yields. These materials are also used in this study. However, since the triangular and square strip geometries are quite different, it was decided to re-test many of the same variations tested previously. This choice allows us to verify the yield numbers reported in Ref. [2] since the two tests have uncorrelated systematic errors. Given the final purpose of this R&D, we have called our test module the preshower prototype module.

Figure 3 shows the actual triangular tile cross-section as fabricated. A so-called *normal* strip is a right isosceles triangle of base 9 mm and height 4.5 mm. A slot 1.5 mm deep and 0.75 mm wide is milled in the base of the triangle, with a 0.75 mm (0.030″) end mill. A second pass is taken along the slot, this time with a 1.07 mm (0.042″) diameter ball end mill, set at a depth such that the

4

bottom of the ball was 1.5 mm below the surface of the scintillator. The tile was flipped over and the triangle cross-section grooves were cut. These grooves are called separation grooves, since they separate adjacent strips within a tile. The amount of scintillator remaining at the nadir of the separation grooves to connect adjacent strips was 0.008".

Except when otherwise noted, the standard fiber used is 0.835 mm diameter Kuraray multi-clad Y-11 with a concentration of 350 ppm. In addition, multi-clad Y-11 250 ppm fiber and Bicron BCF-91A single-clad fiber were also tested. Except as noted, each fiber was 1.5 meters long and had one end diamond polished and silvered by vacuum deposition. Each fiber was threaded through a fiber groove and the silvered end made flush with the edge of the scintillator. A single drop of "five minute" epoxy was placed at each end of the scintillator to keep the fiber in place. Thus, one meter of the fiber is surrounded by scintillator (although separated by an air gap) and 0.5 meters of fiber extends from the scintillator.

A total of 16 different variations were tested, each containing 8 strips. These variations were:

350 Unsilvered This variant used BC-404 scintillator, normal strips, and Y-11 350 ppm multi-clad fiber. The end of the fiber normally silvered was polished, but no silvering was applied.

250 Unsilvered This variant used BC-404A scintillator, normal strips, and Y-11 250 ppm multi-clad fiber. The end of the fiber normally silvered was polished, but no silvering was applied.

91A Unsilvered This variant used BC-404A scintillator, normal strips, and commercially available Bicron BCF-91A single-clad fiber. The end of the fiber normally silvered was polished, but no silvering was applied.

404 Heated This variant used BC-404 scintillator, normal strips, but the tile was heated enough to soften the scintillator

404 0.038" This variant used BC-404 scintillator, normal strips, except the diameter of the ball mill used was 0.038".

404B Heated This variant used BC-404BL scintillator, normal strips, but the tile was heated enough to soften the scintillator.

404A Normal This variant used BC-404A scintillator, normal strips.

404 0.100" This variant used BC-404 scintillator, normal strips, but the depth of the fiber groove was 0.100".

404 0.050" This variant used BC-404 scintillator, normal strips, but the depth of the fiber groove was 0.050".

404 0.015" This variant used BC-404 scintillator, normal strips, but the amount of scintillator remaining at the nadir of the separation groove was 0.015".

404 0.006" This variant used BC-404 scintillator, normal strips, but the amount of scintillator remaining at the nadir of the separation groove was

5

0.006".

404 Normal This variant used BC-404 scintillator, normal strips.

404B Normal This variant used BC-404BL scintillator, normal strips.

404B Painted This variant used BC-404BL scintillator, normal strips, but the "saw-toothed" side of the scintillator was painted with a white glossy paint.

404B 1 Black This variant used BC-404BL scintillator, normal strips, but a black stripe was drawn to reduce inter-channel crosstalk (details in Sec. (3.1)).

404B 2 Black This variant used BC-404BL scintillator, normal strips, but two black stripes were drawn to reduce inter-channel crosstalk (details in Sec. (3.1)).

The triangular profile was made by using a 45° end mill and making a series of successively deeper cuts, until the desired small amount of scintillator remained (0.006", 0.008", 0.015"). The achieved triangular profile (Fig. 3) differs from the ideal (Fig. 1) in two notable features: the flat spot at the peak of the triangle and at the nadir of the separation groove. The flatness at the peak of the triangle is caused because scintillator of 4.5 mm thickness was used. The thickness of the scintillator at the bottom of the separation groove would need to be zero in order to remove this flat spot. It should be noted that this flat spot is not present if a 0.25" (6.35 mm) thick scintillator plate were used, as this scintillator is thick enough to accommodate the 4.5mm triangle and the scintillator remaining below the separation groove. The cause of the flatness at the nadir of the separation groove is simply the width of the cutting surface of the mill. Neither of these flat regions substantially affect the performance of the detector.

The large tiles consisting of 40 (BC-404BL), 24 (BC-404A), and 64 (BC-404) strips of scintillator were then separated into smaller tiles, each consisting of 8, one meter long, triangular strips. Each tile contained only strips of a particular detector variant and was wrapped in commercially available 0.0007" aluminum foil, with the shiny side nearer the scintillator. During wrapping, an unused tile was used to force the foil to conform to the saw-toothed edge of the wrapped tile. Were this not done, it would have been difficult to snugly combine two tiles as shown in Fig. 3.

After saw-toothed sides of two tiles were placed together as shown in Fig. 3, the two tiles were taped together. The result is a mega-tile with a trapezoidally shaped cross-section. The eight trapezoidal mega-tiles were stacked vertically and placed in a holder which both kept the mega-tiles from moving and provided alignment (this stack is shown in Fig. 4). The fiber from each strip was placed in a black Delrin connector and the fibers were then potted with Bicron BC-600 optical glue. After the glue had cured, the end of the connector was diamond finished to a glass-like luster. The design of the connector used

is discussed in Ref. [8]. It is the same type used by the DØ Fiber Tracking Group in their cosmic ray test stand.

3.1   Special Preparation

A few of the detector variants required special handling. These were:

404B Painted The saw-toothed side of a tile was painted with acrylic latex white gloss paint. Care was taken to ensure that the paint did not pool in the bottom of the separation grooves. Several coats were applied.

404B 1 Black An otherwise normal tile of BC-404BL was placed on a flat surface, fiber groove side up. Using a straight edge, an approximately 1 mm wide stripe was drawn using an ordinary permanent black magic marker directly beneath the nadir of each separation groove. Care was taken to ensure that each line was truly black. If insufficient care was taken, the black lines were translucent.

404B 2 Black Black stripes were drawn as in the **404B 1 Black** case and the tile was flipped over so the saw-toothed side pointed up. Then a second black line was drawn along the flat nadir of the separation grooves. Care was taken to keep the black line away from the sides of the triangles.

Heating Machined tiles were placed in an oven at 225° F and heated until soft. This was tested by placing a small piece of scrap scintillator near the machined tiles and checking its hardness periodically. The tiles were not heated enough to have a significant permanent deformation.

4   Test Stand

The DØ Fiber Tracking Group's cosmic ray test stand has been discussed in Ref. [2,9]. Briefly, ribbons of scintillating fibers, planes of Iarocci tubes and standard scintillating paddles provide a trigger and very precise tracking. By embedding some of the scintillating trigger paddles between and below thick steel slabs, one may apply two different momentum thresholds by requiring hits in different combinations of scintillator paddles. For the data set in this paper, it was required that the energy of the cosmic ray exceed 0.8 GeV. We define a coordinate system with z parallel to the fiber, pointing away from the readout end, y pointing up, and x running transverse to the scintillating strips in the direction required to form a right-handed coordinate system. Because the x measurement is done with the scintillating fiber ribbons, the x resolution of tracks projected to our test module was 120 μm. The z measurement was done by the Iarocci tubes and the z resolution of tracks projected to our test module

was 500 μm.[2] Triggering and tracking restrictions yield a distribution of track slopes, Gaussian-like in character, with RMS values $(\Delta x/\Delta y)_{\mathrm{rms}} = 0.057$ and $(\Delta z/\Delta y)_{\mathrm{rms}} = 0.376$.

The 128 channels of the preshower prototype module are connected to a bundle of 8 meter long, clear multi-clad Kuraray [6] fibers, each of which transports light to a separate VLPC. The signal from each VLPC is then electronically amplified, digitized, and read out in the Fiber Tracking Group's normal data stream.

5 Data Set and Results

Data was taken in May 1995. After requiring the cosmic ray tracks to pass through the fiducial volume of the detector, 520 000 events were available for subsequent analysis—approximately 60 000 events per strip. The digitized signals from each strip were corrected for known amplifier non-linearities (as discussed in Ref. [2]).

The most important consequence of using the triangular strip geometry is the improved position resolution. However, as eq. (2) suggests, three parameters must first be accurately determined before the position resolution can be stated. These are: (1) the position of the strips relative to one another, (2) the rotation of the strips with respect to known axes, and (3) the light yield of each strip for a particle travelling through the maximum thickness of scintillator.

5.1 Uniformity of Response Along Strip Direction

Uniformity of response along the strip direction is affected by several things. Variations in scintillator light generation and the conversion of that light in the WLS fiber are often negligible effects, a fact which seems to be true for this analysis as well. A third effect is the attenuation length of the WLS fibers. Both silvered and unsilvered fibers were used in different detector configurations. This was done in large part to verify the substantial effect that silvering has on the response uniformity along the strip direction. In order to measure this quantity, tracks were projected into the preshower prototype and the hit strips determined.[3] The tracks were required to be nearly vertical in xy projection

---

[2] The position resolutions reported here differ slightly from that reported in Ref. [2] due to minor changes in the fiber tracker hardware and in the tracking software.
[3] In a typical event, 16 strips were hit (see Fig. 4).

$(|\frac{\Delta x}{\Delta y}| < 0.02)$. No requirement on the yz slope of the tracks was made. For this measurement, hits were integrated over the entire transverse dimension of the hit strips (i.e. the tracks were only required to be within 4 mm of the center of the hit strips in the x direction). This cut was applied independently for each strip.

In order to reduce the effect of mis-measured tracks at the ends of the detector, the hit strip was required to have a signal of at least two photoelectrons. Because of the high light yield of the strips (discussed in Sec. (5.3)), this rejects no events which actually hit the strip, but rejects those events which, due to the yz resolution of the tracker, are inaccurately reported as hitting a strip. Finally, in order to reduce the effect of any possible slope-dependent trigger bias, the light yields were corrected for differences in path length. Since particles not at normal incidence traverse more scintillator, on average they generate larger signals. Multiplying by $\cos\theta$, where θ is the angle of the track measured with respect to the normal of the mega-tile, removes this effect.

Figure 5 contains a plot of this average slope-corrected yield as a function of z for two randomly chosen fibers (while the plot shows two specific fibers, the slopes are entirely representative). Both silvered and unsilvered fibers are shown. Both curves have been normalized to unity at $z = 0$ (the readout end). While this choice of normalization clearly shows the improved uniformity with silvered fibers, it masks the fact that in addition, silvering also improves the overall yield. This fact is addressed in Sec. (5.3).

If one normalizes the response to unity at $z = 0$ as suggested above and determines the average response over the entire meter of scintillator, one finds an average response of 94.4% with an RMS of 3.4% (for silvered fibers). Because this variation in response is small, for all subsequent analyses no binning in z is done. The variation for unsilvered fibers is larger but for comparison purposes, the analysis on this fiber type is unbinned as well.

5.2   Uniformity of Response Transverse to Strip Direction

Since light generation is proportional to the amount of scintillator traversed, it is expected that when the number of photoelectrons observed in a strip is plotted as a function of position transverse to the strip length, a triangular profile should be observed. This expectation is complicated by the fiber groove, which will reduce the average signal when a particle crosses this region. Figure 6 shows such a plot for a randomly chosen strip. In generating this plot, the data was analyzed as described in the preceding section and no cut on the z position of the track was made beyond requiring $100 < z < 900$ mm.

Several features of Fig. 6 should be noted. The first is the nearly triangu-

lar shape. Secondly, the presence of the fiber groove is clearly evident. As expected, the extent to which the fiber groove causes deviation from the nominal triangular behavior is proportional to the milled depth of the fiber groove. It is also evident that the fiber groove is not always perfectly centered on the triangular cross-section. This has no discernible effect on any important detector performance result.

The final feature to note is the deviation from triangular behavior at distances approximately ± 4.5 mm from the nominal center of the strip. This effect is expected, given the flattened groove between the triangular strips (see Fig. 3). This effect will be revisited in Sec. (5.5).

5.3   Yield

The triangular geometry complicates the task of determining the light yield of each strip. Since the yield is proportional to the amount of scintillator traversed, the question must be cast in a way which reflects this effect. The plots discussed in the previous section were used. Each plot was fit to a triangular function with a base of 9 mm and a height of 4.5 mm. Three free parameters were used in the fit: (1) the position of the peak of the triangle with respect to an externally defined coordinate system (δ), (2) the yield of the strip in units of photoelectrons per millimeter of scintillator traversed (Y), and (3) the amount of scintillator left below the separation groove (ϵ). This last term reflects the fact that the depth of the separation groove varied. The fit was done over the restricted regions (2 mm $< |\Delta x| <$ 4 mm), where Δx is defined to be the distance of the track from the nominal strip center. Excluding the center mitigated the effect of the fiber groove.

The results, presented in Table 1, were much as expected, although they did contain some surprises. Comparing the values of ϵ for the **0.015"** variant and the **0.008"** variants gives the expected $\epsilon_{0.015"} - \epsilon_{0.008"} = 0.007"$. However, $\epsilon_{1 \text{ Black}} - \epsilon_{0.008"} \simeq -0.003"$. This is interpreted as the black stripe absorbing light that would have otherwise been converted in the WLS fibers. Since this absorption would increase as the track approached the black stripes, the net effect is to modestly alter the fit. Otherwise, the black stripes have limited effect on the yield.

One of the most striking features is the lateral shift of the top and bottom tile with respect to one another within a mega-tile. This shift is small, typically smaller than 400 μm but, as we shall see in Sec. (5.4) and Sec. (5.6), this can have large effects. Figure 3 would lead one to believe naively that the peak of a triangle in the top layer would be naturally aligned with the nadir of the separation groove of the bottom layer. However, the holder used in this test

squeezed the mega-tiles from the left and right. If a small amount of vertical space is available, this allows the two tiles to move with respect to one another as seen in Fig. 7. Such an effect was not anticipated during detector design, but we expect to be able to remove it using somewhat different construction techniques. The amount of shift between top and bottom layers within a mega-tile is given in Table 1.

The yield in units of photoelectrons per millimeter of scintillator traversed is broadly as expected. These results are also given in Table 1. As a cross-check, a fit was done to the plots discussed in Sec. (5.2), using two independent lines in the region of $(-4 \text{ mm} < \Delta x < -2 \text{ mm})$ and $(2 \text{ mm} < \Delta x < 4 \text{ mm})$ respectively (Δx as above). The intercept of these two lines was found and the result divided by the nominal thickness (4.5 mm). The yield results determined by the fit to a triangle function and the fit two independent straight lines agree with an RMS of 3%.

The signal actually measured is the number of photoelectrons. The desired measurement is WLS photons from the strips. These photons must cross an optical connector, 8 meters of 0.965" diameter clear multi-clad fiber, another optical connector, and finally be converted from photons to electrons in the VLPC's. All of these stages reduce the final signal. The best known of these effects is the attenuation length of the clear fiber (10.4 ± 0.5 meters) [10]. This reduces the signal by $e^{-8/10.4}$. More poorly known are the transmission efficiencies at the couplers ($\sim 90\%$) and the quantum efficiency (QE) of the VLPC pixels ($\sim 65\%$). These effects were investigated by injecting known amounts of light into the connectors and VLPC's. An attempt is made to correct for transmission and QE effects on a channel by channel basis, but the residual variation from these effects is estimated to be $\sim 15\%$. Since this variation tends to be common to a detector variant, one is not helped by the eight independent channels of a particular variant (i.e. eight adjacent channels are similar, but groups of eight might be quite different).

Thus in determining the WLS photons from the observed number of photoelectrons, one must multiply the QE corrected signal by 4.1 ± 0.6. [4] As expected, the unsilvered fibers give less yield than the silvered ones, but beyond that, it is difficult to make strong statements about the relative yields of different detector variants, although one may say that they are roughly equal at the 15% level.

---

[4] Note: $4.1 = [\exp(-8/10.4) \times 0.90 \times 0.90 \times 0.65]^{-1}$

5.4 Uniformity in Yield Across a Mega-tile

While the cross-section of individual strips is triangular, as Fig. 1 shows, each normally incident particle traverses a constant amount of scintillator, regardless of its impact point. Thus adding properly normalized signals from the top and bottom layers should give a constant response. Defining S^{max} to be the amount of signal generated by a particle travelling through the maximum amount of scintillator (in practice this is the yield determined in Sec. (5.3) multiplied by 4.5 mm of scintillator), one can then define

$$S^{\mathrm{total}}_{\mathrm{normalized}} = S_{\mathrm{top}}/S^{\mathrm{max}}_{\mathrm{top}} + S_{\mathrm{bottom}}/S^{\mathrm{max}}_{\mathrm{bottom}}$$

and plot this quantity as a function of the position where the track intercepts the scintillator layer. Such a plot is shown in Fig. 8.

The most evident feature is the fact that the plot is not as flat as expected. In addition to the understandable fiber grooves, there appears to be a cyclical non-uniformity. The cause of this non-uniformity is the shift between the top and the bottom layers of a mega-tile (discussed in Sec. (5.3)). As is apparent in Fig. 7, there is a variation in the amount of thickness of scintillator traversed. The magnitude of this effect is given by Δ_N, the deviation from nominal. This quantity can be given as:

$$\Delta_N = 1 \pm \frac{\delta}{a}$$

where δ is the shift of the top layer with respect to the bottom layer, and $2a$ is the base of the triangular strip. Thus a shift of 0.45 mm corresponds to a 10% non-uniformity in response. It is therefore imperative that the relative inter-layer alignment between the top and bottom layer of a mega-tile be very nearly nominal (i.e. $\delta \sim 0$). We expect that a minor change in the construction techniques will yield better alignment.

5.5 Crosstalk Between Adjacent Strips

As seen in Fig. 3, adjacent strips within a tile are connected by a small strip of scintillator. This strip of scintillator allows a fraction of the light generated in one strip to be seen in its neighbor. Define the strip through which a charged particle passes to be the central strip and define the two strips on either side of the central strip within a tile to be adjacent strips.[5] Further define the

---

[5] Note that the edge strips (strips #1 and #8 in an eight strip tile) have only one adjacent strip.

proportionality constant k via the expression k = (average photoelectrons in adjacent strip)/(average photoelectrons in central strip).

Ref. [11] outlines a method for determining k by plotting the average number of photoelectrons in the adjacent strip as a function of the number of photoelectrons observed in the central strip. Mathematically, one can say:

$$< \sigma(\Sigma) > = k \frac{\int_0^\infty e^{-S} S^{\Sigma+1} f(S) \, dS}{\int_0^\infty e^{-S} S^{\Sigma} f(S) \, dS} \tag{3}$$

where $f(S)$ is the distribution of the average number of photoelectrons in the central strip (S) (this is different from the distribution of the observed number of photoelectrons, a point which will be addressed below), Σ is the observed number of photoelectrons in the central strip and $< \sigma(\Sigma) >$ is the average number of photoelectrons in the adjacent strip as a function of Σ. It should be noted that generally k is, strictly speaking, not a constant. As charged particles cross closer to the edge of a strip, the probability of seeing a signal in an adjacent strip increases. In this analysis, we ignore this effect and report the average crosstalk.

Eq. (3) shows that if one can determine $f(S)$, then k can be determined in a straightforward way. The distribution $f(S)$ is not directly accessible. What one may observe is $\mathcal{F}(\Sigma)$, the distribution of observed number of photoelectrons in the central strip. These two functions are related via the expression

$$\mathcal{F}(\Sigma) = \int\limits_0^\infty f(S) e^{-S} S^{\Sigma} \, dS / \Sigma! \tag{4}$$

Thus $\mathcal{F}(\Sigma)$ is simply the function $f(S)$ smeared by Poisson statistics.

One may determine $f(S)$ using Monte Carlo techniques in the following way. First, randomly choose the position where a particle crosses the triangularly shaped central strip and determine the thickness of the scintillator crossed. Next, using Landau theory, choose an amount of energy lost by the particle (ΔE) and thus generate a distribution $f(\Delta E)$. Since S is directly proportional to ΔE, by scaling $S = C \, \Delta E$, the distribution $f(S)$ is achieved. The constant C is found to be 19.6 pe/MeV; this comes from the ratio of the average number of photoelectrons generated for a particle crossing the maximum thickness of scintillator (18 photoelectrons in 4.5 mm of scintillator) to the average energy lost in the same thickness of scintillator (0.92 MeV).

This distribution $f(S)$ may be verified by inserting it into eq. (4) and finding $\mathcal{F}(\Sigma)$. When the $\mathcal{F}(\Sigma)$ distributions so obtained are compared with data, good agreement is obtained.

13

To extract the k's, a similar analysis was performed. Because the fractional crosstalk increases when a track passes near the edge of a strip, only events in which the charged particle passes within 3.2 mm of the center of the central strip are used. Further, the usual requirement of vertical tracks ($|\Delta x/\Delta y| <$ 0.02) is imposed. The data and the Monte Carlo were treated identically.

The theory curve (eq. (3) after inserting $f(S)$) resulting from this approach was fit to the data as a one parameter (k) fit (see Fig. 9). The crosstalk for each channel both into the next higher number and the next lower number strip was separately determined. The small systematic discrepancy between fit and data above 17 photoelectrons is likely due to a small error in the derived $f(S)$ function and has little effect on conclusions drawn here.

The k's so determined are not quite the desired quantity. What is really desired is a ratio k' which is the (amount of light in the adjacent strip)/(the amount of light in the central strip). It is possible for neighboring strips to have slightly different photoelectron yields for an identical amount of light and thus one must correct for this effect via $k' = \left(S_{\text{central}}^{\max} / S_{\text{adjacent}}^{\max} \right) k$.

One expects that most of the crosstalk comes from light which undergoes many reflections inside the central strip before passing through the narrow channel left by the separation groove. This randomization of the photon's direction suggests that the amount of crosstalk should be simply related to the depth of the separation groove compared to the total thickness of scintillator.[6] In addition, the presence or absence of the black stripes in the separation groove should affect the amount of crosstalk. Because we have several pairs of adjacent strips for each detector variant, we are able to determine the crosstalk measured for each pair and look at the distribution of crosstalk constants. Table 2 tabulates the results. This table includes the expected crosstalk, which is merely the ratio of the thickness of scintillator below the separation groove to the total scintillator thickness. In addition, the table lists the mean (the average crosstalk for that geometry), the RMS (the spread of crosstalk's achieved for that geometry) and standard error (RMS divided by the square root of the number of samples) of the actual crosstalk measured.

The observed results have some important expected features, although in general more crosstalk is observed than expected. Less scintillator remaining below the separation groove decreases crosstalk. Similarly, the presence of the black stripe(s) decreases crosstalk. A notable oddity is the **404B Painted** variation, which has little crosstalk. The cause of the unexpectedly high amount of crosstalk for the other variations is not known, but we speculate that a likely cause may be that the aluminum foil does not perfectly follow the surface of the separation groove and possibly some light crosses the air gap above the

---

[6] $k_{\text{expected}} = $ (thickness of scintillator left by the separation groove)/(total thickness of scintillator).

connecting scintillator strip. The painted surface blocks this light path, thus reducing inter-strip crosstalk.

5.6 Position Measurement Resolution

One of the main reasons for investigating triangular cross-section strips is to use light sharing between adjacent strips within a mega-tile to attain a position resolution that is much better than the strip-to-strip separation. Equation (2) shows how one can determine the track position with respect to the strip's center. Using the yield numbers of Sec. (5.3) to determine the S^{max}'s, one can make a profile plot of the x position as determined by the triangular strips (x_{vernier}) as a function of the actual track position as determined by the test stand tracker (x_{actual}). An example of this plot is given in Fig. 10a. This plot is for a randomly chosen strip in a plane with a $\delta = 0.215$ mm. As can be seen, there is a systematic deviation between x_{vernier} and x_{actual}. Similarly, when a residual ($x_{\mathrm{vernier}} - x_{\mathrm{actual}}$) is calculated, the RMS is ~ 1 mm, as shown in Fig. 10b.

The cause of the systematic deviation is the shift between the top and bottom layers of a mega-tile, first discussed in Sec. (5.3). As seen in Fig. 7, one effect of this shift is to make the vernier effect asymmetric, that is, the effective size of the vernier triangles on the left differs from the size of those on the right. This effect can be expressed mathematically by changing eq. (2) to

$$x_{\mathrm{vernier}} = x_o + \delta \pm (a \mp \delta)\frac{S_2/S_2^{\mathrm{max}}}{S_1/S_1^{\mathrm{max}} + S_2/S_2^{\mathrm{max}}} \tag{5}$$

In essence, a has been replaced by $a \mp \delta$, where δ is the inter-tile shift (a signed quantity), and this small shift δ is added. This equation assumes that the peak of the reference triangle is exactly at x_o. Further, this equation is rigorously true only in those regions where the thickness of scintillator traversed by normally incident particles is uniform (i.e. the "flat" sections in the thickness curve of Fig. 7b).

Using eq. (5) removes the systematic effect seen in Fig. 10a. Figure 11a shows the corrected plot of x_{vernier} against x_{actual}. When a residual is formed (Fig. 11b), the RMS of the residual distribution is typically 580 μm. Figure 12 shows the distribution of resolutions for all strips. After excluding strips with unsilvered fibers and also "edge" strips (i.e. strips #1 and #8 in an 8 strip tile), the distribution of resolutions is peaked at 580 μm, with an RMS of 20 μm. The unsilvered fibers are excluded due to their lack of uniformity in z and their much reduced photostatistics. The end strips are unusual due to the fact that they do not have two neighbors and are therefore intrinsically

15

asymmetric.

This resolution includes the intrinsic detector resolution, but also includes effects due to misalignment, errors in yield determination, and tracking resolution. Due to the large statistics in the data set, it is possible to determine (a) the position of each strip to 10 μm and (b) the yields to within 3%. The mis-measurement of the yields has an effect which is difficult to characterize in a simple manner. This point is perhaps best illustrated by an example. Assume that in eq. (2) S_2^{max} is mis-measured by 3% and S_1^{max} is known perfectly. Then when S_2 is small, the mis-measurement is affecting a small quantity and has little effect. Similarly, when S_2 is large, this mis-measurement occurs in both the top and the bottom of the fraction, again having a small effect, due to self-normalization. Thus the biggest effect of this yield mis-measurement occurs at an impact position of $x = a/2$, relative to the center of the strip which defines the origin. If one assumes that one strip was mis-measured 3% high and the other 3% low, the maximum effect on the resolution is 60 μm. Averaging over the entire strip, one finds an average addition to the resolution of 40 μm.

Finally, the resolution of the fiber tracker for tracks projected to the preshower prototype is 120 μm and the effects of multiple scattering are negligible. Subtracting these three contributing effects in quadrature from the measured resolution of 580 μm, one finds an intrinsic detector position resolution of 567 μm.

Using $< S_{\mathrm{max}} > = 20$ photoelectrons and the results detailed in Fig. 2, the resolution should be approximately 450 μm. This neglects the effects of Landau fluctuations. As discussed in Sec. (2), when Landau fluctuations are included, the predicted resolution is 560 μm, in excellent agreement with the data.

6   Summary of Results

An extensive study of triangular cross section scintillating strips with WLS fiber and VLPC readout has been performed. Yields of 4 photoelectrons per millimeter of scintillator traversed have been achieved, in good agreement with earlier studies. The most important new property is the improved position resolution for tracks crossing adjacent strips. We have achieved 567 μm, using triangular strips of base 9 mm, height 4.5 mm and with a typical maximum yield of 20 photoelectrons. Using conventional scintillating fiber designs, one would need a detector with a granularity of 2 mm ($\sim \sqrt{12} \times 0.567$ mm) to achieve a comparable position resolution, which can be accomplished only by using twice as many channels. Based on the results presented here, further improvements in the resolution should be attainable by decreasing the size

16

of the base of the triangle, increasing the photostatistics yield or reducing the Landau fluctuations. While Landau fluctuations are unavoidable when charged particles transit matter, what is important is the ratio of the width of the energy loss distribution to the mean. Through a judicious choice of materials and thicknesses, this effect can be minimized. We further note that the position where a particle crosses a fiber is always reported as the center of the fiber (although in the case of multiple layers of fibers it is possible to have better position resolution than the center-to-center fiber spacing of a single layer). The triangle design allows for interpolation, which reduces some of the effects caused by the granularity of a fiber detector. The critical nature of inter-layer alignment within a mega-tile has been shown. Inter-strip crosstalk is shown to be approximately 6%, using black stripes between adjacent strips. Finally, it should be noted that achieving the same position resolution using conventional scintillating fiber designs would be more expensive due to the increased channel count.

Acknowledgement

17

References

[1] R. Wojcik et al., Nucl. Instr. and Meth. A 342 (1994) 416; Proceedings of SCIFI93: Workshop on Scintillating Fiber Detectors, ed. A.D. Bross, R.C. Ruchti, M.R. Wayne, World Scientific Press.

[2] M. Adams et al., Nucl. Instrum and Meth. A, **366**, 263, (1995).

[3] D. Adams et al., FERMILAB-Conf-94/318-E, presented at DPF'94; M. Atac et al., Nucl. Instr. and Meth. A 314 (1992) 56; M.D. Petroff and M.G. Stapelblock, IEEE Trans. Nucl. Sci. **NS-36** (1989) 158; M.D. Petroff and M. Atac, ibid., p. 163.

[4] B. Gomez et al., (DØ Collaboration), FERMILAB-DØUPGRADE-E-823, Oct 1993.

[5] Bicron Corporation, 12345 Kinsman Road, Newbury, OH, 44065-9677, USA. Tel. +1 (216) 564-2251.

[6] Kuraray Intl., 200 Park Ave, New York, NY 10166, USA. Tel. +1 (212) 986-2230.

[7] A. Pla-Dalmau, G.W. Foster and G. Zhang, Volume 1, FERMILAB-TM-1873, December 1993; A. Pla-Dalmau, G.W. Foster and G. Zhang, FERMILAB-TM-1875, December 1993.

[8] S. Margulies and M. Chung, in "Scintillating Fiber Technology and Applications II", ed. E. J. Fenyves, Proc. SPIE, Vol. 2281, pp. 26-34, 1994.

[9] D. Adams et al., FERMILAB-Conf-94/312-E, presented at DPF'94; DØ Fiber Tracking Group, *Cosmic Ray Test Results of the DØ Prototype Scintillating Fiber Tracker*, FERMILAB-CONF-95-012-E, to be published in the proceedings of the 4th International Conference on Advanced Technology and Particle Physics, Como, Italy, 3-7 October 1994, Ed. by Z. Borchi.

[10] C.L. Kim, private communication.

[11] D. Lincoln, F. Hsieh, H. Li, Nucl. Instrum and Meth. A, **366**, 277, (1995).

Figure Captions

1. A diagram of an ideal mega-tile with definitions of the most salient quantities in eq. (1).
2. The best resolution achievable as number of photoelectrons varies. The resolution is given in units of a, where $2a$ is the length of the base of the triangle. The horizontal axis is the average number of photoelectrons observed for a charged particle travelling through a hypothetical piece of scintillator T_{max} thick.
3. Actual mega-tile cross-section after manufacturing (a=4.5 mm and T_{max}=4.5 mm).
4. Side view of the test module after all 8 layers were stacked. A representative cosmic ray is seen.
5. The response of two strips as a function of z. Both sets of data were fit to an exponential and then normalized to unity at $z = 0$. The fits are superimposed as lines. Closed circles denote unsilvered fibers and open squares denote silvered fibers.
6. An example of the response of a strip as a function of the distance a charged particle passes from the strip's axis. The solid curve is a fit to a triangle function, with the two regions indicated simultaneously entering the fit.
7. (a) Effect of a slight (10%) lateral shift of one tile with respect to another within a mega-tile. (b) A diagram of the thickness of scintillator a charged particle traverses as a function of impact position. Note that the variation in thickness due to the fiber grooves is not included.
8. (a) An example of the normalized total signal for a particle crossing a mega-tile with a large shift (0.466 mm) between the two tiles within a mega-tile. (b) An example of the normalized total signal for a particle crossing a mega-tile with a small shift (0.033 mm) between the two tiles within a mega-tile. In both figures, the horizontal line indicates perfectly uniform response (after the strip-to-strip normalizations have been applied). In both plots, the position of the fiber grooves is indicated by the arrows.
9. A fit of the observed crosstalk data to a theoretical curve. The solid circles denote data, and the crosses denote theory. The fit is restricted to the region indicated on the plot. For this example, the amount of crosstalk is 14.8%.
10. (a) The position reported by the prototype module as a function of actual impact position of the charged particle, without accounting for the inter-tile shift. The superimposed line denotes a perfect correlation. (b) Distribution of residuals before the inter-tile shift correction.
11. (a) The position reported by the prototype module as a function of actual impact position of the charged particle, after accounting for the inter-tile shift. The superimposed line denotes a perfect correlation. (b) Distribution of residuals after the inter-tile shift correction.
12. Distribution of the resolution achieved for all strips. The hatched histogram includes only "good" strips (i.e. exclude edge strips and strips with unsilvered fibers). The hatched and unhatched areas added together give the

distribution of resolutions achieved for all strips.

Detector Variation	Shift (mm) (±0.03)	Yield (pe/mm)
350 Unsilvered	—	2.54 ± 0.05
91A Unsilvered	0.212	1.74 ± 0.03
250 Unsilvered	—	2.17 ± 0.08
404 Heated	0.466	4.01 ± 0.06
404 0.038"	—	3.67 ± 0.05
404B Heated	0.033	3.74 ± 0.10
404A Normal	—	3.28 ± 0.09
404 0.100"	0.369	3.89 ± 0.16
404 0.050"	—	3.92 ± 0.08
404 0.015"	0.296	3.67 ± 0.10
404 0.006"	—	3.97 ± 0.08
404 Normal	0.424	3.88 ± 0.13
404B Normal	—	3.75 ± 0.13
404B Painted	0.141	4.25 ± 0.13
404B 1 Black	—	3.47 ± 0.14
404B 2 Black	0.215	3.47 ± 0.08

Table 1
Each pair of detector variants are the two tiles that made up a specific mega-tile. The shift column shows the distance one tile is shifted with respect to the other within the mega-tile. The yield column shows raw average yield, before corrections for effective quantum efficiency. The error quoted contains both statistical and systematic effects.

Detector Type	Number of Samples	Expected Crosstalk (%)	Average Crosstalk (%)	RMS Crosstalk (%)	Standard Error Crosstalk (%)
0.008"	108	4.51	14.85	2.08	0.20
0.015"	14	8.47	20.17	1.29	0.35
0.006"	14	3.39	10.36	2.09	0.56
Painted	14	4.51	6.06	1.52	0.41
1 Black	10	—	9.93	1.64	0.52
2 Black	14	—	6.06	2.08	0.56

Table 2
Detector variants with similar crosstalk characteristics are grouped together. Crosstalk fractions k both into the next higher numbered and next lower numbered strips are calculated and the measured mean, RMS and standard error for each crosstalk variant are reported here. When a model exists, the expected crosstalk is given. In all cases, the actual crosstalk exceeds expectations.
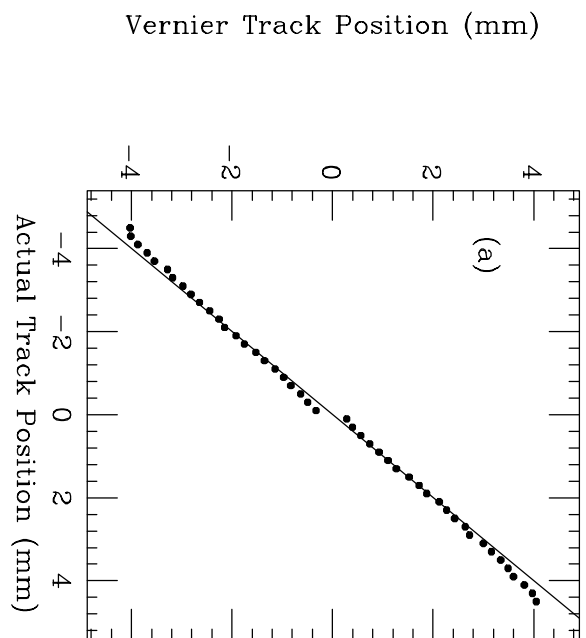
Figure 1
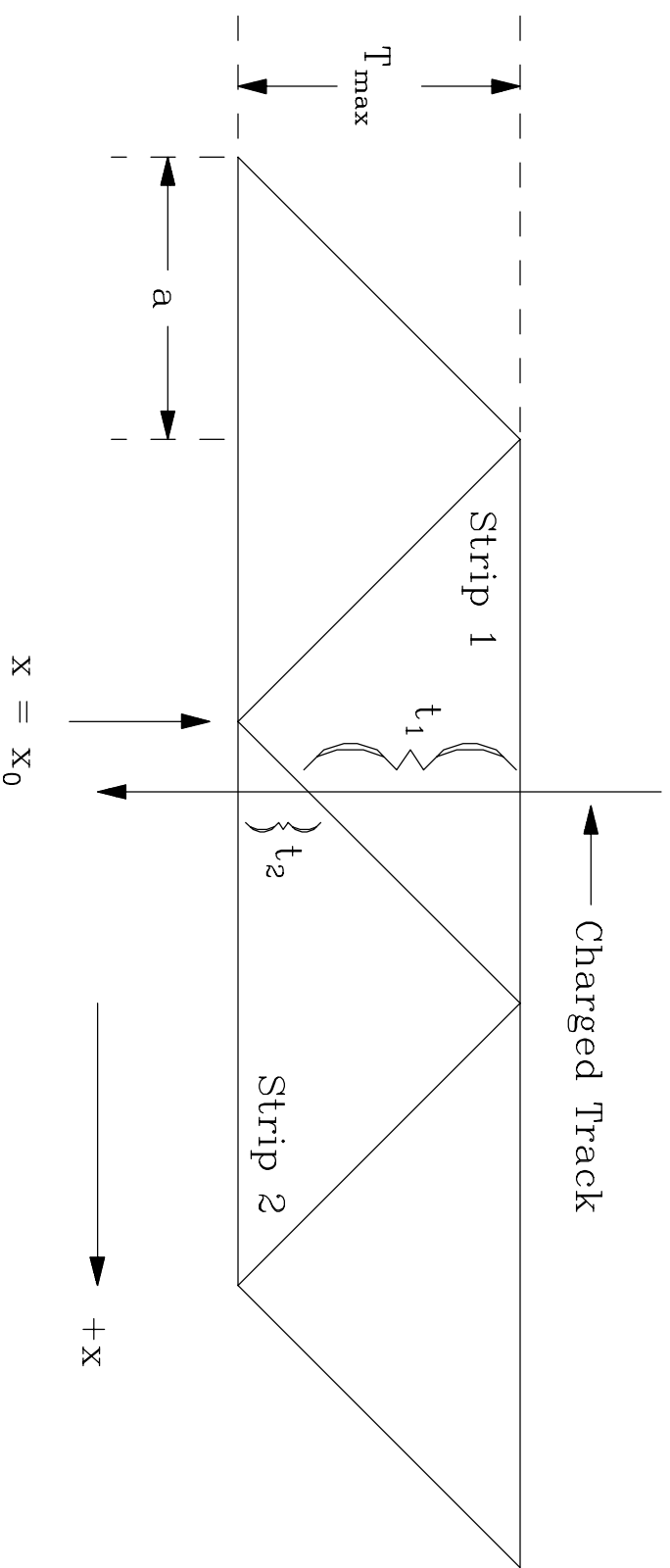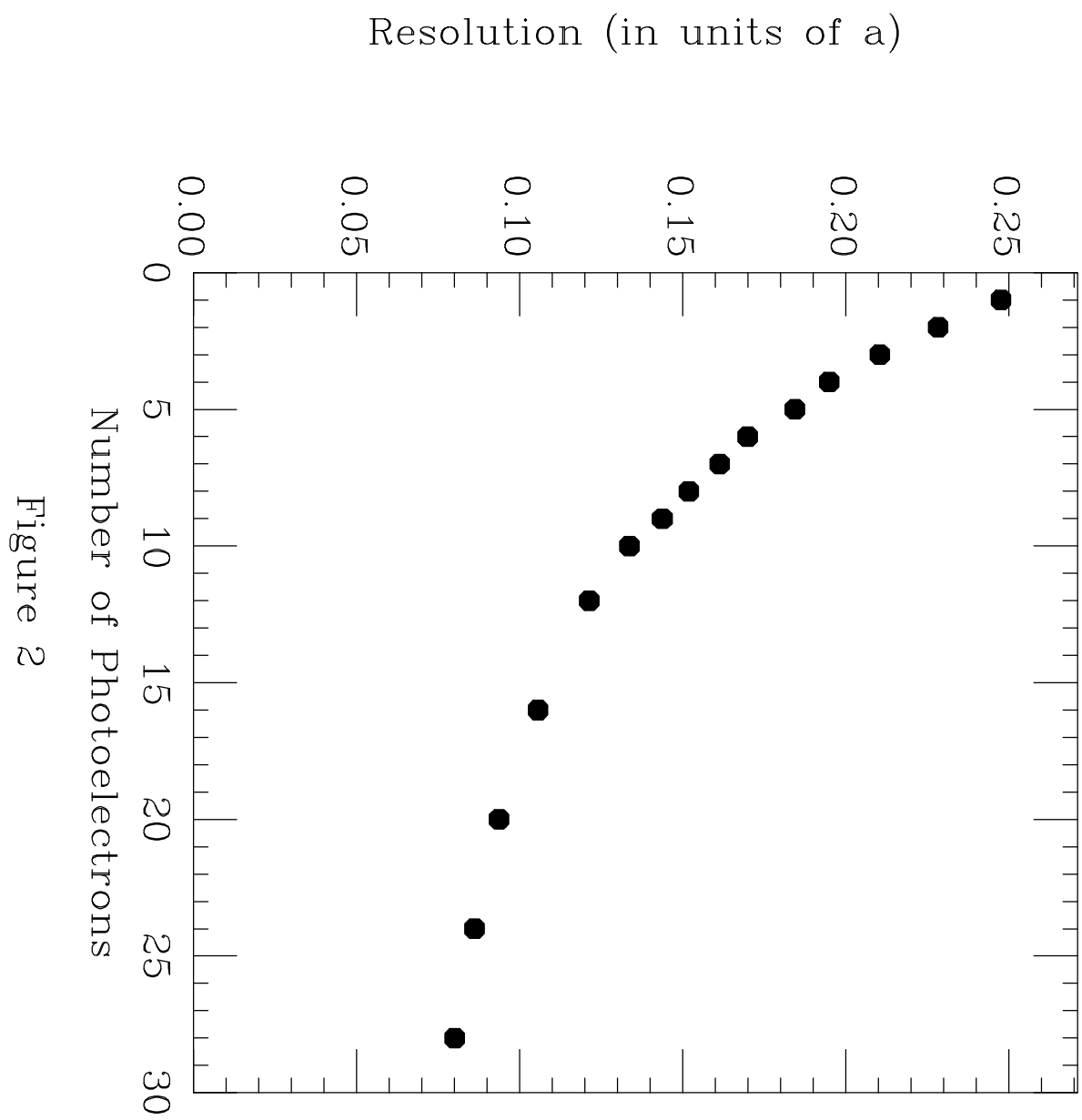
Figure 2

Figure 3

Figure 4

Representative Track

Figure 5

Figure 6

T_max

a

δ

(a)

Thickness

T_max

Position

(b)

Figure 7

Figure 8

Figure 9

Number of Events

Vernier Track Position (mm)

(b)

(a)

$X_{vernier} - X_{actual}$ (mm)

Actual Track Position (mm)

Figure 10

Number of Events

Vernier Track Position (mm)

(a)

Actual Track Position (mm)

(b)

$X_{vernier} - X_{actual}$ (mm)

Figure 11

Figure 12